A New Metric to Measure Shape Differences in fMRI Activity

Siddharth Khullar*[1,2], Andrew M. Michael[2], Nicolle Correa[3],
Tulay Adali[3], Nathan Cahill[1], Stefi A. Baum[1], Vince D. Calhoun[1,2,4]

1. Chester F. Carlson Center for Imaging Science, Rochester Institute of Technology, Rochester, NY,
2. Mind Research Network, Albuquerque, NM
3. University of Maryland, Baltimore County, Baltimore, MD
4. University of New Mexico, Albuquerque, NM

ABSTRACT

We present a novel shape metric for quantification of shape differences between the spatial components obtained from independent component analysis (ICA) of group functional magnetic resonance imaging (fMRI) data. This metric is utilized to measure the difference in shapes of the activation regions obtained from different subjects within a group (healthy controls or patients). The parameters comprising the metric are computed for each pixel on the outermost contour (edge) of an activation region for each slice. These parameters are in the form of (r, θ) pairs that may be interpreted as the length and orientation of a vector originating from the centroid of the activation region to the pixel belonging to the boundary contour. Using this information we extract three features that quantify the shape difference between the two shapes under observation. The reference and observation shapes may be selected in two ways: (a) activation maps from two different subjects or (b) mean activation map compared against subject-wise activations, as obtained from group ICA. We present different methods to visualize the shape differences, thus providing a tool to observe the spatial differences within a group or across groups. In addition to the above results, we also address a few special cases where two or more activation contours are present in a single slice and present potential solutions for accounting for these regions as special measures. Our results show that this metric has utility in creating a better understanding of the variability in brain activity among different groups of subjects performing the same task.

Keywords: fMRI, shape metrics, group ICA

1. INTRODUCTION

One of the key results obtained from analyzing group data in an fMRI study is to estimate the spatial maps that indicate the locations and magnitudes of brain activity. The neural activity recorded in form of fMRI data sets is usually represented using a *t*-test or a *z*-score measure. These maps are derived at a subject level and/or at the group (control or patient) level as a mean map. Depending on the method used for fMRI data analysis, e.g. via a general linear model (GLM) or ICA, it is possible to obtain multiple spatial maps for a single subject in addition to a group map. GLM [1, 2] is a regression method which utilizes 2-level analysis model to calculate beta weights, contrasts and *t*-maps for each subject and each condition at the first level and perform a 1-sample *t*-test on the first level data from all subjects to estimate the group maps for each condition at the second level. On the other hand, ICA [3, 4] is a data-driven method that clusters functionally correlated voxels into various segmented maps, commonly known as functional networks. Unlike the GLM, ICA works independently of a temporal model. Thus, ICA has the ability to derive functional clusters of voxels that may remain uncovered when using GLM. These functional networks may or may not be related to the task but are useful for deriving functional network connectivity, that is, the correlation between different networks in the brain within a subject or across the whole group.

Numerous techniques have been introduced in the past to quantify the shape of planar and volumetric objects (see [5, 6] for a comprehensive survey). The seminal paper by Freeman [7] introducing chain codes was one of the first methods proposed for quantifying shapes of line drawings and images. Since then, shape representation methods have been grouped as (1) contour-based and (2) region-based methods. Contour-based methods like chain codes [7], Fourier descriptors [8], autoregressive models [9], and chain code based shape numbers [10] utilize the boundary information which is essentially similar to how humans perceive and compare complex shapes. Region-based methods such as Zernike moments [11] and grid-based shape measures [12] exploit local shape information such as centroid, major and minor axes-based measures. The proposed method in this paper belongs more to the latter class and is simple to

Medical Imaging 2011: Image Processing, edited by Benoit M. Dawant, David R. Haynor,
Proc. of SPIE Vol. 7962, 79624K · © 2011 SPIE · CCC code: 1605-7422/11/$18 · doi: 10.1117/12.878219

understand and implement than most other complicated metrics. The metric proposed in this paper is a function of different parameters explained later.

In this paper, we introduce a novel weighted metric estimated from a given 2-D shape by utilizing polar distances and orientations of several pixels on its contour. Centroid based measures have been previously utilized in combination with B-splines for applications in object recognition and detection [13, 14], but there have only been a few attempts made to quantify the shape of activations in fMRI data [15-17] , and most fMRI papers utilize existing complex shape descriptors. Here, we present a simpler technique that utilizes polar measures of closed 2-D contour(s) that comprise a 3-D shape across multiple axial slices.

The paper is organized as follows. Section 2 describes the various methods, type of fMRI data and processing steps involved. Results are presented in Section 3 along with relevant discussions followed by conclusions in Section 4.

2. METHODS

In functional brain imaging, the underlying shape of an activation region (spatial) determined from statistical analysis is an important characteristic which should be preserved. Shape of the activated regions is usually distorted due to the several preprocessing and analysis steps involved in detecting neural activity and bring out the underlying spatial ROI related to the BOLD activation. Most fMRI studies involve investigating neural activity in one or more group of subjects and it can be useful to quantify the spatial differences within or across two groups through measuring and comparing shapes of the spatial activation regions. The purpose of this paper is to provide tools that can quantify the shape variation that exists between subjects and enable researchers to gain more information about the spatial nature of BOLD fMRI activations.

In this section, we explain the functioning of our proposed metric in addition to details regarding the fMRI data, experimental paradigm, preprocessing and analysis. A detailed block diagram is presented in Fig. 1 which illustrates all the major steps involved in fMRI processing leading to application of our proposed metric towards the end.

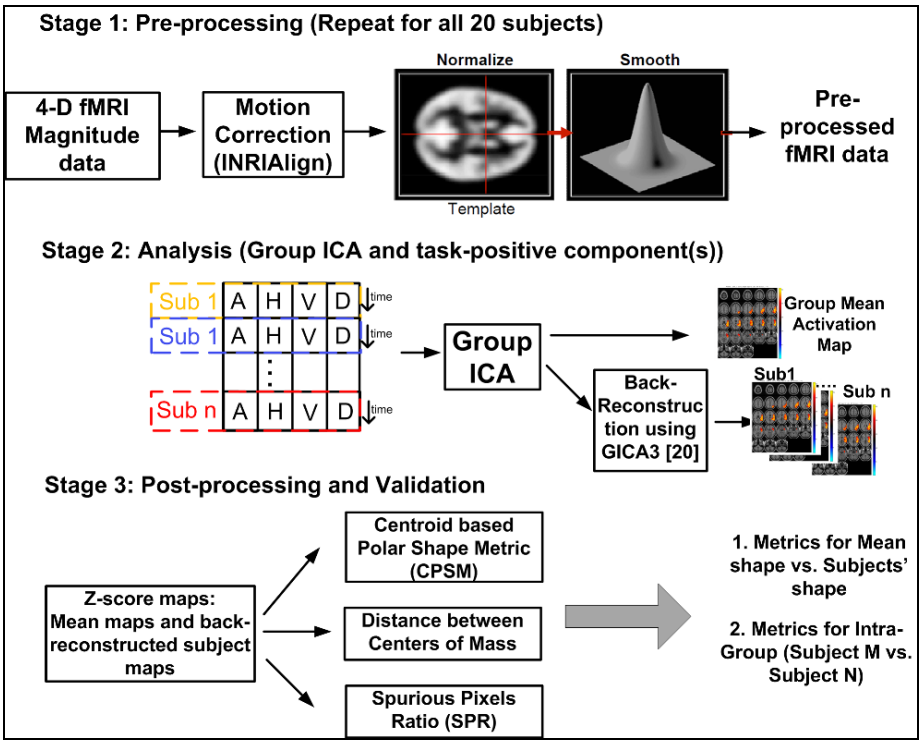

Figure 1: The block diagram showing the basic ICA-based fMRI processing stages along with application of the proposed shape metric.

2.1 fMRI Subjects and experimental paradigm

We implement our method on data obtained from twenty healthy subjects while they in a motor tapping experiment, 17 subjects were right-handed, and 3 subjects were left-handed and in the age group between 18 and 62 years, with 12 male subjects and 8 female subjects. IRB-approved informed consent at the University of New Mexico was obtained from all the participants. The finger-tapping fMRI task is a block-design (ON/OFF) with periods of 30 s off and 30 s on. The subjects tapped their right-hand fingers during the ON period and rested during the OFF cycle. A single run of the experiment comprised of five and half cycles, starting with off and ending with off period. For each subject, 165 whole head fMRI images were collected while they performed a single run of the experiment inside the scanner. Steps were taken to ensure that all participants could hear the stimuli and discriminate them from the background scanner noise.

2.2 Image acquisition and pre-processing

All imaging was performed on a 3-T Siemens Total Imaging Matrix (TIM) system with a 12-channel radio frequency (RF) coil. The scanning parameters are as follows: field of view (FOV) = 24 cm, slice thickness = 3.5 mm, slice gap = 1 mm, number of slices = 32, matrix size = 64 × 64, TE = 29 ms, TR = 2 s, flip angle = 70˚. About 165 whole head fMRI images were acquired and analyzed, and the first 6 images discarded to allow for stabilization of T1 effects.

The fMRI magnitude images (initially recorded as real and imaginary parts separately) were estimated and written as 4D NIfTI (Neuroimaging Informatics Technology Initiative) files for further analysis. Preprocessing of the data was performed using the SPM5 software package (http://www.fil.ion.ucl.ac.uk/spm/software/spm5/). Images were motion corrected using INRIAlign [18] to compensate for head movement in the fMRI time series images. Following that, all image volumes were spatially transformed by registering them to Montreal Neurological Institute (MNI) space using the echo-planar imaging (EPI) template built into the SPM5 package. Next, the original data with a voxel size of $3.75\times3.75\times4.5$ mm^3 is re-sampled to $3\times3\times3$ mm^3 and this resulted in $53\times63\times46$ voxels per volume using bilinear interpolation. Lastly the data are spatially smoothed, using a Gaussian smoothing kernel of size $8\times8\times8$ mm^3.

2.3 Centroid-based Polar Shape Metric (CPSM)

The proposed shape metric is briefly described and applied specifically to simulated fMRI data for comparison of different image smoothing algorithms [19]. First, we include more features and present its application to task-based group fMRI data that involves measuring differences between activation shapes in different subjects at a finer level. Some of these features include counting pixels for absent regions in either of the activation maps under consideration. Second, we also take into account the distance between the centroids of the activation clusters from the template and source maps. Finally, here we apply the method to subject data, In [19] we previously presented results of the shape metric using simulated data. In such cases, the ground truth is available in contrast to real data sets. Since the spatial properties of activation regions vary considerably in different subjects, it is useful to compare the shapes for every subject against the shape of the mean activation map as well as the shape of activation in other subjects. The details of the centroid-based polar shape metric (hereafter CPSM) are explained below followed by description of some additional features that add to the power of existing metric and provide additional information about the difference between spatial shapes of individual subject's neural activity.

In order to compare two shapes, the metric uses edge maps extracted from the task-positive Z-score component maps (right somatosensory motor cortex) obtained after group ICA. As mentioned before, these maps can either correspond to any two subjects or to the mean activation and a subject, depending on the comparison being done. The model order for ICA was set to 20 [3, 19]. The threshold for extracting these binary maps was set to be three standard deviations, that is, a Z-value of 3 or greater. Four main error measures are utilized to estimate the parent metric value. Additionally, other parameters mentioned above are computed and combined with the parent metric to yield the final CPSM value.

Algorithm for Computing CPSM:

STEP 1: Initiate the algorithm with the edge maps for reference (subject X's or mean activation) and observation (subject Y): Z_{ref}^{edge} and Z_{obs}^{edge} as the inputs. Estimate the variable size vectors containing locations of edge pixels in the i^{th} slice: e_{ref}^{i} and e_{obs}^{i}. Apply steps 2-7 to slices containing activation common to both input maps.

STEP 2: Compute the centroid coordinates - c^i_{ref} for the i^{th} slice through Z^{edge}_{ref}. Estimate the polar coordinates (r, θ) for each pixel in e^i_{ref} and e^i_{obs}, with c^i_{ref} as the origin of the coordinate system, and stored as (r^i_{ref}, θ^i_{ref}) and (r^i_{obs}, θ^i_{obs}).

STEP 4: Locate /count the pixels in e^i_{obs} whose (r, θ) match perfectly with pixels of e^i_{ref} in a pair wise manner. The total count of these pixels is termed as the ***gain*** - α^i.

STEP 5: Locate/count the pixels in e^i_{obs} whose r estimates only match perfectly with pixels in e^i_{ref}. Thus, these pixels contribute to rotational (angle) error, given they are in the same angular quadrant (see Fig. 2). This error primarily accounts for all pixels that have shifted away from the line joining it to the centroid. These errors are recorded in form of MSE values $\omega^{MSE}(i)$ for i^{th} slice:

$$\omega^{MSE}(i) = \frac{1}{N_{err}} \sum_{k=1}^{N_{err}} (\theta^i_{obs}(k) - \theta^i_{ref}(k))^2 \tag{1}$$

where $k \in (1,2,3,.....,N_{err})$ corresponds to the indices of pixels with a rotational error in slice i.

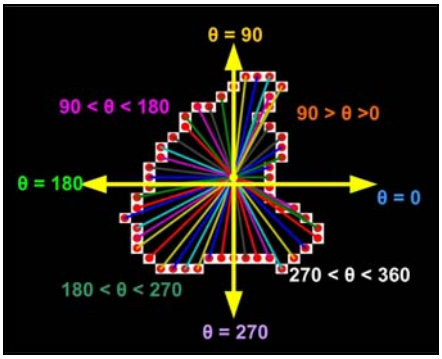

Figure 2: Illustration for computation of rotational and translational errors in each quadrant as explained in Steps 3 – 5**.** Vectors from the Centroid to each pixel are depicted in different colors along with clearly labeled axes. Various angular quadrants are also labeled to better understand the angular errors and decision criteria.

STEP 6: Locate /count the pixels in e^i_{obs} whose θ estimates only match perfectly with pixels in e^i_{ref}. Thus, these pixels contribute to translational (distance) errors that may have occurred due to a pixel moving along the line joining it to the centroid. These errors are recorded in form of MSE values ($\delta^{MSE}(i)$) for each slice i:

$$\delta^{MSE}(i) = \frac{1}{N_{err}} \sum_{k=1}^{N_{err}} (r^i_{obs}(k) - r^i_{ref}(k))^2 \tag{2}$$

If a set of corner pixels or pixels in a cusp area in the reference shape are rotated or translated outwards or inwards due to variability in response in different subjects or as a result of different smoothing operations, then these errors are recorded by the metric through the above explained features. A more detailed illustration of these cases can be found in our previous work [19]

STEP 7: Count the number of pixels in e^i_{obs} that neither have a distance match nor an angle match with any of the pixels in e^i_{ref}. This count is stored as a *penalty*: β^i. This error accounts for a large shift of several pixels or addition of a false contour (see Fig. 1(b)).

After obtaining four features for each slice (α^i, β^i, ω^i and δ^i), in the form of four vectors, we proceed to estimate a weighted combination of these in order to represent the shape of a volume with a single number. We initiate this process by projecting each feature vector to a normalized sub-space by scaling each element with maximum value within that vector, resulting in values ranging between 0 and 1. Further, the normalized feature vectors: $\hat{\alpha}^i$, $\hat{\beta}^i$, $\hat{\omega}^i$ and $\hat{\delta}^i$ are accumulated through a weighted sum across each slice resulting in a metric for each slice (see Eqn. 3). This final metric value (*CPSM*) for the given volume is computed by summing across the aforementioned weighted metric vector.

$$CPSM = \sum_{i=1}^{N_{slices}} \frac{2\hat{\delta}^i + \hat{\omega}^i + \hat{\beta}^i}{2\hat{\alpha}^i} \quad (3)$$

where CPSM represents the proposed 'centroid-based polar shape metric'. The above *CPSM* for a given slice is expected to have a low value when the number of perfect matches ($\hat{\alpha}^i$) is high and the value of the penalty ($\hat{\beta}^i$) is low and there are low values for errors - $\hat{\delta}^i$ and $\hat{\omega}^i$. The coefficients/weights were set based on the significance of the type of error. Perfect matches are always weighted the highest and assigned as the denominator, reducing any bias that could be introduced due to a high number of penalty pixels (β^i) for a given slice.

After having obtained the CPSM, we continue to estimate a few more parameters that are useful in validating the behavior of CPSM for various subjects and also useful on its own. These parameters are:

*Distance between centers of mass (**DCM**):* This parameter is estimated for the two 3-D shapes under comparison as the Euclidean distance between the centroids of the 2 shapes under comparison. The results for this measure are illustrated in Fig. 3 and Fig. 4 below. This measure enables the user to determine whether the center of mass of activation in a particular subject was anatomically close to mean activation or close to activation of another subject. This measure can easily be converted to MNI space to find the exact anatomical locations and assist in making detailed inferences about the BOLD activity.

*Spurious pixels ratio (**SPR**)*: A common problem in handling threshold maps is getting rid of regions/pixels of no interest. Such pixels are usually termed as 'spurious' pixels. Usually, these regions are removed using morphological opening or closing. In this paper, we utilize this information by the counting the number of pixels in each of the threshold images under comparison. For example, the mean activation map and each subject's activation map can have different number of regions/pixels that do not belong to the primary activation cluster that is used to measure CPSM. The ratio may be expressed as:

$$SPR^i = \frac{N^i_{\text{subject}}}{N_{\text{mean}}} \quad (4)$$

Where N^i_{subject} is the number of spurious pixels in i^{th} subject's activation map and N_{mean} is the number of spurious pixels in the group mean map. This ratio can be greater than 1 in the case $N^i_{\text{subject}} > N_{\text{mean}}$ which indicates that there were more spurious pixels in the subject's image indicating neural activity elsewhere that may be well be worth investigating further for that subject. In Eqn. 4, the quantity N_{mean} can be replaced with N^j_{subject} which is the number of spurious pixels in j^{th} subject's activation map in order to estimate the SPR between two different subjects. In the next section we present some applications and results from applying the proposed shape metric on a real fMRI data set (described in Section 2.1 and 2.2).

3. RESULTS AND DISCUSSION

The utility of the shape metric described in this paper are highlighted using two different applications derived from a single group of subjects. The metric can be utilized in many different ways that are briefly stated later in this section.

3.1 Group Mean vs. Individual Subjects

Frequently, ICA-based fMRI studies typically compare two groups based on their mean maps, but often ignore the variations between individual subject's back-reconstructed ICA activation components and the aggregate maps, which can contain important information. In Fig. 3(a), we present the CPSM results measured by setting the task-positive (motor cortex) group mean component as the reference (see Eqns. 1 – 3) image and setting each subject's back-reconstructed activation map [20] as the observation image. It is clear from Fig. 3(a), that about 8 out of 20 subjects have a CPSM value ≈ 20. This indicates that shape of the activations in these subjects is relatively close to the mean activation map. The lowest CPSM value was obtained for subject 3 ≈ 19 units whereas subject 12 is estimated to be the most different in shape with a CPSM value ≈ 86 units. In order to visualize the difference in shape, a few slices of the activation maps are overlaid on an anatomical image of the human brain as shown in Fig. 3(b). Significant differences

and similarities can be observed in the shapes of subject 12 and subject 3 respectively. There are definitely more 'red' pixels signifying areas that show neural activity in subject 12 but not in case of the mean map ('black pixels'). Similarly, the shape of subject 3's activation region is closely related to the shape of the mean activation. Other differences such as shift in centers of mass and activity in spurious or non-task significant areas is accounted for by the distance between centers of mass (DCM) and spurious pixels ratio (SPR) measures.

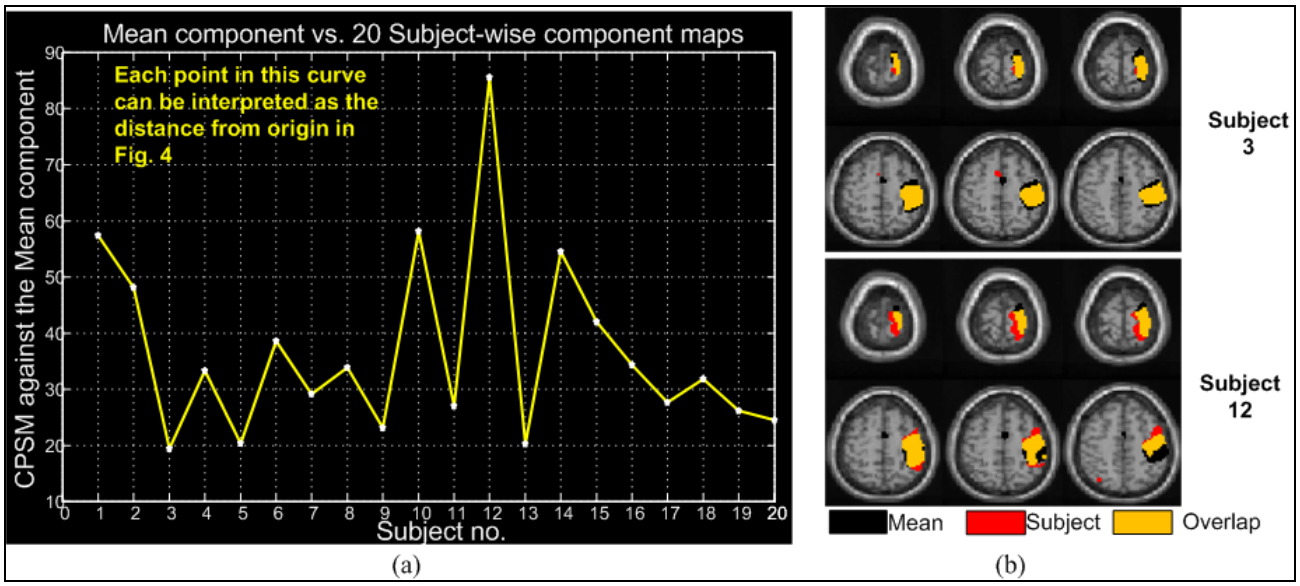

Figure 3: CPSM values obtained by comparing the group mean activations against subject specific maps – (a) Curve showing variation in shape of activation across 20 subjects when compared against the shape of the group mean map. (b) Overlaid maps of subject 3 (lowest CPSM) and subject 12 (highest CPSM) to illustrate the spatial features that result in difference in shape. Note that there are more red voxels (subject activation only) in subject 12 than in subject 3 indicating large variation in activation contours of the former.

4.1.1. The 'Orbital' Graph

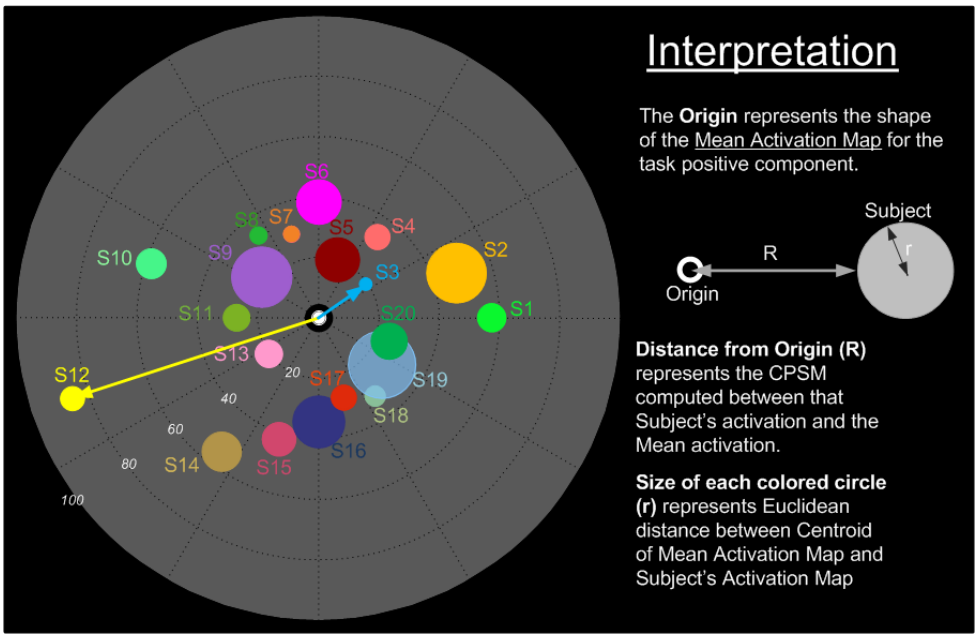

Figure 4: An orbital curve showing absolute shape differences across the group versus the mean using CPSM and DCM measures. As explained in the key on the right, farther the circular region, higher the CPSM value (see Fig. 3). Each circle corresponds to a different

subject (arranged in a counter-clockwise manner starting from subject 1 (S1)) whereas the radius of circles represent a scaled DCM measure. A large circle indicates that the activation cluster for that subject was centered at a far away voxel as compared to the activation cluster in the group mean map.

Fig. 4 is an orbital representation of the variation between different subjects and the mean. The origin in this representation (white circle in Fig. 4) signifies the mean activation map and is considered as the reference point for all other subject specific activation maps. In this figure, we incorporated the DCM measure (described as *r* in Fig. 4) along with the CPSM values estimated for every subject. Note that circles are arranged in a counter-clockwise manner, increasing from 1 to 20. The radius of the colored circles representing each subject (as annotated) is a scaled DCM value whereas the orbit marked as 0 – 100 in steps of 20 represents the number of CPSM units (described as *R* in Fig. 4) that subject is different from the mean. The circles with centers between 0 and 30 correspond to the subjects whose shape is closest to the shape of the mean activation in terms of CPSM units. This graph provides an overall view of the difference between the mean activation and different subjects. Such an orbital graph can be created with any subject's activation map set as the reference image and compared to other subjects' activation shapes. Also, this graph incorporates the CPSM and the DCM measure into a single method to visualize the variation between various subjects.

As seen from Fig. 4, subject 3 has the closest center of mass to the mean center of mass (DCM = 0.6 pixels) whereas subject 19 that corresponds to the largest circle in Fig. 4 has a DCM value = 3.25 pixels. Even though the CPSM values for subject 3 (~ 19 units) and subject 19 (~ 26 units) are low, the difference between their DCM values can provide significant information relating the activation centers for this particular task positive component. The actual values of the CPSM represented in Fig.4 as the location of circles are also presented in Fig. 3(a) for easier interpretation.

The next measure presented here is the spurious pixels ratio (SPR) as described in Eqn. 4. SPR was computed using the mean activation map and individual subject maps and is presented in Fig. 5. All subjects that have high SPR values can be considered worth analyzing individually for some interesting task-related activations in regions that are not a part of the motor cortex. Here, the subjects 2, 5, 8, 11, 14, 17 and 20 have very high SPRs indicating large number of non-ROI pixels being active in these subjects in comparison with the non-ROI pixels that are active in the mean component.

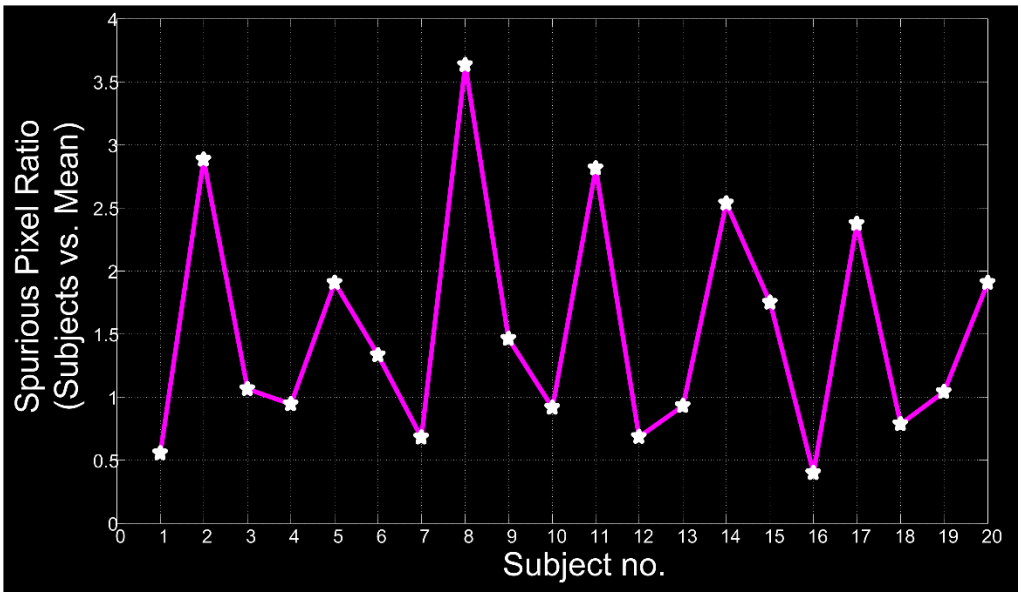

Figure 5: Variation in the SPR measure (see Eqn. 4) across various subjects. Subjects 2, 5, 8, 11, 14, 17 and 20 have high SPRs indicating that there exist relatively large regions that are not a part of the primary activation region (motor cortex).

3.2 Intra-group Comparisons (Subject *i* vs. Subject *j*)

After having quantified the group level mean activation maps with the back-reconstructed maps for individual subjects, we present some subject-to-subject comparisons that are in agreement with the pattern seen in Figs. 3 and 4 when

comparing the mean activation with each subject. The subjects that have a low CPSM value in group comparison show low values here when put against subjects that had a high CPSM value (see Fig. 6). We present the subject-to-subject CPSM values (see Fig. 6) as a stacked bar plot where each subject (along the x-axis) is compared with every other subject (colored blocks in each bar). Note that, the colored block representing the subject used as reference will be missing from the bar corresponding to the same subject since the metrics are equal to zero when comparing them with each other.

In Fig. 6, we summarize the intra-group comparisons where each subject is compared against every other subject on the basis of shape, that is, the CPSM. Note the large size of color blocks corresponding to subject 12 as compared to all other subjects, this verifies the observations made for subject 12 in Figs. 3 and 4. The large CPSM measures for subject 19 against other subjects may be accounted by the fact that the activation for this subject was the farthest from the mean, thus resulting in high values for the distance parameter δ^{MSE} (Eqn. 2) and the gain and penalty measures that comprise the CPSM metric. Subjects 1, 10, 12, 14 are the other subjects that correspond to the highest cumulative values in Fig. 6, this is consistent with the peaks seen in Fig. 3 and the circles lying in the outer orbits in Fig. 4.

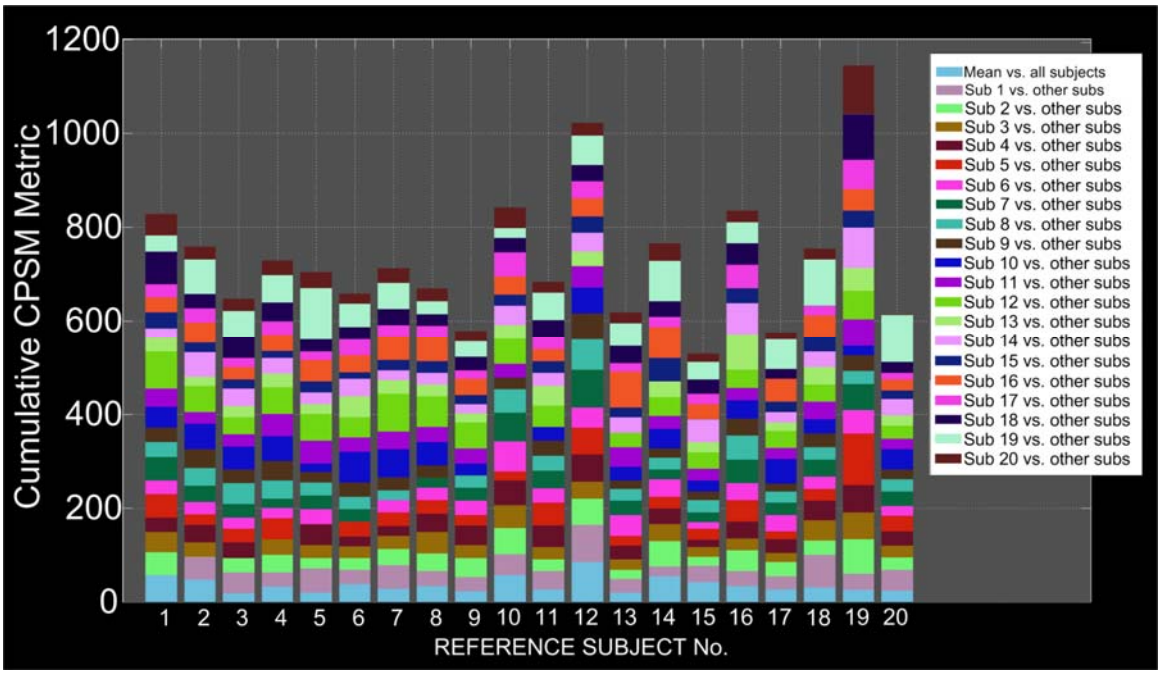

Figure 6: Illustration of subject-to-subject variations obtained by comparing each subject's activation shape against every other subject. Each color block (along y axis) represents the CPSM value when compared against the Reference Subject (x-axis). The lowest row of color blocks represent the difference from mean (same information as Fig. 3a) with subjects 1, 10, 12 and 14 showing large values (see color legend for mean). Note that these subjects are the ones with highest cumulative CPSM values in this graph (tallest bars) subjects suggesting a large overall difference from rest of the subjects.

The SPR and DCM measures for within-subject comparisons can be estimated in a similar way but are not presented here due to limitations of space. When there is a need to compare two or more subjects (and not all subjects) within the same group for some specific differences in activity, researchers might benefit by estimating subject-to-subject differences in SPR and DCM.

As seen from this section, the proposed metric can be utilized in many different ways to quantify changes in activation shapes within and across groups. In addition to the utilities illustrated here, there are other possible uses depending on the data being used for group analysis such as (1) comparison between different analysis and fMRI pre-processing methods; (2) comparing patient groups and variation in neural activity under different conditions of brain state (while engaged in a cognitive task or while at rest); and lastly (3) using the shape metric as a potential feature in addition to amplitude of fMRI activation, temporal and spectral difference for measuring variability across large scale resting state fMRI group studies [21].

As mentioned earlier, a useful application of this shape metric can be comparing preprocessing methods as presented in our recent work [19]. In that paper, we illustrated the distortion effects of various denoising schemes on shapes of activation regions using simulated fMRI data. We were able to compare the changes in shape more specifically since the ground truth was available for the simulated neural activity. This is not the case for real task-fMRI or resting state fMRI data. For real fMRI data, it is typically necessary to track changes in neural activity at a group level and generate useful statistics to make strong comparisons. The proposed shape metric measures could be easily utilized to add to the power of existing statistical measures and measure the changes across subjects within the same group. Another possible application can be to compare various functional networks that co-exist during different states of the brain, that is, while at rest or performing a task. It has been shown that several such networks co-exist within the same group of subjects while they do a task or while at rest [22]. The differences in shapes of these activation regions associated with different networks can be a useful measure to make an estimate of the differences in location of neural activity which in turn can assist in making other unknown inferences about the human brain. Large scale resting state studies have revealed differences in various functional domains based on various features such as gender, age and ethnicity [21, 23]. The shape metric feature can also reveal significant spatial differences while acting as additional information to the existing set of features.

4. CONCLUSIONS

In this paper we illustrate that shape of the activation regions across different subjects in a group varies considerably and, if accounted for, can be utilized itself as a useful feature for comparison. We present a new metric that is able to quantitatively measure the difference between activation regions through a single numeric value in addition to a few supplementary features such as DCM and SPR that can be used to learn more about the detailed differences between any two shapes. To summarize, this metric presents a potential feature that would help explain the dynamics of fMRI activity across different subjects in a single study or across different studies. The new metric proposed in this paper may help neuroscience researchers build a better comparison model between subjects based on the shape of their activation regions and also help classify these differences based on other features such as age, sex and ethnicity. This metric can also act as a training feature for design of SVM and neural networks used for separating artifacts from BOLD-related components when using ICA for signal separation. Also, we believe this shape metric will prove to be a useful tool for comparison of different pre-processing methods used for preparing fMRI data for further analysis.

REFERENCES

[1] K. Friston, A. Holmes, K. Worsley *et al.*, "Statistical parametric maps in functional imaging: a general linear approach," Human Brain Mapping, 2(4), 189-210 (1994).

[2] S. Huettel, A. Song, and G. McCarthy, [Functional magnetic resonance imaging] Sinauer Associates Sunderland, MA, (2004).

[3] V. Calhoun, T. Adali, G. Pearlson *et al.*, "A method for making group inferences from functional MRI data using independent component analysis," Human Brain Mapping, 14(3), 140-151 (2001).

[4] V. Calhoun, T. Adali, G. Pearlson *et al.*, "Spatial and temporal independent component analysis of functional MRI data containing a pair of task related waveforms," Human Brain Mapping, 13(1), 43-53 (2001).

[5] J. Tangelder, and R. Veltkamp, "A survey of content based 3D shape retrieval methods," Multimedia Tools and Applications, 39(3), 441-471 (2008).

[6] D. Zhang, and G. Lu, "Content-based shape retrieval using different shape descriptors: A comparative study." 1139-1142.

[7] H. Freeman, "Computer processing of line-drawing images," ACM Computing Surveys (CSUR), 6(1), 57-97 (1974).

[8] E. Persoon, and K. Fu, "Shape discrimination using Fourier descriptors," Systems, Man and Cybernetics, IEEE Transactions on, 7(3), 170-179 (2007).

[9] H. Kauppinen, T. Seppanen, and M. Pietikainen, "An experimental comparison of autoregressive and Fourier-based descriptors in 2D shape classification," Pattern Analysis and Machine Intelligence, IEEE Transactions on, 17(2), 201-207 (2002).

[10] E. Bribiesca, and A. Guzman, "How to describe pure form and how to measure differences in shapes using shape numbers," Pattern Recognition, 12(2), 101-112 (1980).

[11] W. Kim, and Y. Kim, "A region-based shape descriptor using Zernike moments," Signal Processing: Image Communication, 16(1-2), 95-102 (2000).
[12] G. Lu, and A. Sajjanhar, "Region-based shape representation and similarity measure suitable for content-based image retrieval," Multimedia Systems, 7(2), 165-174 (1999).
[13] R. Gaborski, and J. Paskali, "A Cognitively motivated video detection system," Journal of Applied Science & Engineering Technology, 1(0), (2007).
[14] E. Saber, Y. Xu, and A. Murat Tekalp, "Partial shape recognition by sub-matrix matching for partial matching guided image labeling," Pattern Recognition, 38(10), 1560-1573 (2005).
[15] F. Yang, and Z. Shan, "Mapping developmental precentral and postcentral gyral changes in children on magnetic resonance images," Journal of Magnetic Resonance Imaging, 33(1), 62-70 (2011).
[16] J. Looi, M. Walterfang, M. Styner *et al.*, "Shape analysis of the neostriatum in frontotemporal lobar degeneration, Alzheimer's disease, and controls," NeuroImage, 51(3), 970-986 (2010).
[17] A. Scher, Y. Xu, E. Korf *et al.*, "Hippocampal shape analysis in Alzheimer's disease: a population-based study," NeuroImage, 36(1), 8-18 (2007).
[18] L. Freire, and J. Mangin, "Motion correction algorithms may create spurious brain activations in the absence of subject motion," NeuroImage, 14(3), 709-722 (2001).
[19] S. Khullar, A. Michael, N. Correa *et al.*, "Wavelet-based fMRI analysis: 3-D denoising, signal separation, and validation metrics," NeuroImage, (2010).
[20] E. Erhardt, S. Rachakonda, E. Bedrick *et al.*, "Comparison of multi-subject ICA methods for analysis of fMRI data."
[21] E. A. Allen, E. B. Erhardt, E. Damaraju *et al.*, " A baseline for the multivariate comparison of resting state networks," Frontiers in Systems Neuroscience, In press, (2010).
[22] V. Calhoun, K. Kiehl, and G. Pearlson, "Modulation of temporally coherent brain networks estimated using ICA at rest and during cognitive tasks," Human brain mapping, 29(7), 828-838 (2008).
[23] B. Biswal, M. Mennes, X. Zuo et al., "Toward discovery science of human brain function," Proceedings of the National Academy of Sciences, 107(10), 4734 (2010).